Peroxisome Degradation by Microautophagy in *Pichia pastoris*: Identification of Specific Steps and Morphological Intermediates

Yasuyoshi Sakai,* Antonius Koller,* Linda K. Rangell,‡ Gilbert A. Keller,‡ and Suresh Subramani*

*Department of Biology, University of California, San Diego, La Jolla, California 92093-0322; and ‡Pharmacological Science, Genentech, South San Francisco, California 94080

Abstract. We used the dye *N*-(3-triethylammonium-propyl)-4-(*p*-diethylaminophenylhexatrienyl) pyridinium dibromide (FM4-64) and a fusion protein, consisting of the green fluorescent protein appended to the peroxisomal targeting signal, Ser-Lys-Leu (SKL), to label the vacuolar membrane and the peroxisomal matrix, respectively, in living *Pichia pastoris* cells and followed by fluorescence microscopy the morphological and kinetic intermediates in the vacuolar degradation of peroxisomes by microautophagy and macroautophagy. Structures corresponding to the intermediates were also identified by electron microscopy. The kinetics of appearance and disappearance of these intermediates is consistent with a precursor–product relationship between intermediates, which form the basis of a model for microautophagy. Inhibitors affecting differ-

ent steps of microautophagy did not impair peroxisome delivery to the vacuole via macroautophagy, although inhibition of vacuolar proteases affected the final vacuolar degradation of green fluorescent protein (S65T mutant version [GFP])-SKL via both autophagic pathways. *P. pastoris* mutants defective in peroxisome microautophagy (*pag* mutants) were isolated and characterized for the presence or absence of the intermediates. These mutants, comprising 6 complementation groups, support the model for microautophagy. Our studies indicate that the microautophagic degradation of peroxisomes proceeds via specific intermediates, whose generation and/or processing is controlled by *PAG* gene products, and shed light on the poorly understood phenomenon of peroxisome homeostasis.

Protein degradation in eukaryotic cells occurs in the cytosol and in virtually all subcellular compartments. Lysosomes are involved in two types of autophagic processes (Marzella and Glaumann, 1987; Dunn, 1994). The first, called microautophagy, is the sequestration of small portions of cytoplasm (including organelles) by invagination of the lysosomal membrane or by wrapping of a flap-like protrusion (Dunn, 1994). The second process, called macroautophagy, refers to the sequestration of organelles and cytosol by membranes probably derived from the endoplasmic reticulum to generate autophagosomes (Marzella and Glaumann, 1987) that then fuse with the endosomes or lysosomes to release auto-

phagic bodies that accumulate, and are degraded, within the lysosomes (Dunn, 1994). These processes are present in virtually all eukaryotic cells and constitute the major pathway for the degradation and recycling of cellular proteins (Kovacs et al., 1982).

The autophagic degradation of organelles has been demonstrated in yeasts such as *Saccharomyces cerevisiae*, *Hansenula polymorpha*, *Pichia pastoris,* and *Candida boidinii* (Bormann and Sahm, 1978; Veenhuis et al., 1983; Tuttle et al., 1993; Baba et al., 1994). The autophagosomes involved in macroautophagy have been characterized ultrastructurally in *S. cerevisiae*, and shown to be induced by nutrient deprivation and inhibited by PMSF or by mutations in genes affecting lysosomal proteinases (e.g., proteinase A and B; Baba et al., 1994). The distinct morphology of the autophagic bodies that accumulate under nutrient deprivation conditions has been used to isolate *S. cerevisiae* mutants deficient in the accumulation of these structures. These autophagy (*apg* and *aut*) mutants, belonging to 14 distinct complementation groups, are distinct from the vacuolar protein sorting (*vps*) mutants affecting vacuolar biogenesis (Tsukada and Ohsumi, 1993;

Thumm et al., 1994; Noda et al., 1995; Harding et al., 1996). Genetic and biochemical evidence in *S. cerevisiae* also indicates that the vacuolar protein, aminopeptidase I (API), which is imported from the cytosol to the vacuolar matrix by the cytoplasm-to-vacuole (CVT) pathway, shares components used for macroautophagy (Harding et al., 1996; Scott et al., 1996, 1997). In *H. polymorpha*, peroxisome degradation-deficient (*pdd*) mutants have been isolated and these are impaired in the macroautophaigic degradation of peroxisomes (Titorenko et al., 1995).

Whereas studies with *S. cerevisiae* and *H. polymorpha* have focused primarily on the process of macroautophagy, we have investigated the microautophagic degradation of peroxisomes. We have chosen *P. pastoris* as the model system because it exhibits both macroautophagic and microautophagic degradation of peroxisomes in response to different environmental conditions (Tuttle and Dunn, 1995), making it possible to determine to what extent genes involved in the two types of autophagic processes overlap. *P. pastoris* grows on multiple carbon sources. Upon transfer from glucose to methanol medium cytosolic enzymes (e.g., formate dehydrogenase), peroxisomal proteins (e.g., alcohol oxidase and dihydroxyacetone synthase [DHAS][1]) and the peroxisomes themselves, are induced in order to metabolize methanol. At least 18 (peroxin [*PEX*]) genes encoding peroxins are involved in peroxisome biogenesis and import in both yeast and mammalian cells (Subramani, 1998). Upon shift back from methanol medium to glucose or ethanol media, two distinct autophagic pathways of degradation are activated (Tuttle and Dunn, 1995). A shift from methanol to ethanol medium results in the selective degradation of only peroxisomes but not cytosol by macroautophagy. In contrast, the switch from methanol to glucose triggers degradation of cytosolic and peroxisomal enzymes by microautophagy. In *P. pastoris*, the half-life of DHAS and alcohol oxidase is >3 h in stationary phase cultures maintained in methanol. Upon shift to glucose, however, as much as 80% of alcohol oxidase and DHAS is degraded in <3 h in a process selective for peroxisome degradation (Tuttle et al., 1993). Ultrastructural studies have revealed that in methylotrophic yeasts, the degradation of peroxisomes occurs in vacuoles (Veenhuis et al., 1981, 1983; Gould et al., 1992; Spong and Subramani, 1993; Tuttle et al., 1993). Mutants deficient in glucose-stimulated autophagy (*gsa1* and *gsa2*) are unable to sequester peroxisomes in glucose-adapted cells, but they are proficient in macroautophagy in ethanol-adapted cells. However, mutants lacking the vacuolar proteinases A and B (PrA and PrB) are deficient in the vacuolar degradation steps common to both pathways (Tuttle and Dunn, 1995).

In this study, both the peroxisomes and the vacuole of *P. pastoris* cells were labeled with vital stains, i.e., green fluorescent protein (GFP) tagged with a type I peroxisomal targeting signal (PTS1, consisting of the COOH-terminal peptide, serine-lysine-leucine [SKL]) for peroxisomes and a red styryl dye, FM4-64, for the vacuolar membrane. Using this double-fluorescence labeling technique, we followed microautophagy especially at its early stages, and could dissect the process into several intermediate steps. Mutants defective in peroxisome degradation by microautophagy were isolated and classified according to their morphological phenotypes. These morphological and genetic data form the basis of a model for microautophagy in *P. pastoris*.

Materials and Methods

Materials

N-(3-triethylammoniumpropyl)-4-(*p*-diethylaminophenylhexatrienyl) pyridinium dibromide (FM4-64) was purchased from Molecular Probes, Inc. (Eugene, OR). 1-Methyl-3-nitro-1-nitrosoguanidine (NTG) was from Aldrich Chemical Company, Inc. (Milwaukee, WI). 2,2′-Azino-bis(3-ethylbenzthiazoline-6-sulfonic acid) (ABTS), peroxidase (Type VI-A), and wortmannin were from Sigma Chemical Co. (St. Louis, MO).

Strains and Media

P. pastoris strains used in this study were: STW1 (*arg4, his4*::pTW51 (P_{AOX1}GFP-SKL, *HIS4*) described in Wiemer et al. (1996); STW3 (*arg4, his4*::pTW74 (P_{GAPDH}GFP-SKL, *HIS4*); STK1 (STW3, *pag1*); STK2 (STW3, *pag2*); STK3 (STW3, *pag3*); STK4 (STW3, *pag4*); STK5 (STW3, *pag5*); STK6 (STW3, *pag6*), STK7 (*pep4, prB1, his4*::pTW51 [P_{AOX1}GFP-SKL, *HIS4*]) and SJH242 (*arg4, pex1-2, his4*::[*pex1-ts, HIS4*]; Faber et al., 1998).

P. pastoris cells were grown in yeast extract/peptone/dextrose [YPD] medium (containing 2% glucose, 2% Bactopeptone, and 1% yeast extract), YNM medium (containing 0.67% yeast nitrogen base without amino acids, 0.5% [vol/vol] methanol, 0.05% yeast extract), SD medium (containing 0.67% yeast nitrogen base without amino acids, 2.0% glucose), SM medium (containing 0.67% yeast nitrogen base without amino acids, 0.5% [vol/vol] methanol), or SE medium (containing 0.67% yeast nitrogen base without amino acids, 0.5% [vol/vol] ethanol), supplemented with appropriate amino acids (100 μg/ml for arginine, 100 μg/ml for histidine).

Growth and Labeling of Vacuolar Membranes of Methanol-grown Cells with FM4-64

Cells grown at logarithmic phase in YPD medium were washed once and suspended at an OD_{600} of 0.5–0.6, in YNM medium containing 32 μM FM 4-64 (diluted from a 16 mM stock solution in DMSO), and cultured overnight, during which time FM4-64 reached vacuolar membranes through endocytosis and the culture medium turned color from red to yellowish. For the kinetic analysis, >90% cells showed spherical vacuoles without any invagination.

Fluorescence Microscopy and Morphometric Assay for Microautophagy

Labeled cells were collected by centrifugation and transferred to glucose (SD) or ethanol medium (SE). At the indicated time point, samples (200–500 μl) were collected by centrifugation and placed on ice until observation. The morphologies of vacuoles and peroxisomes were stable for at least 2 h.

For the morphometric and kinetic analyses of the various stages of microautophagy we counted the number of single, rounded vacuoles (Factor A); the number of vacuoles invaginated by a cluster of peroxisomes (Factor B); the number of vacuoles having double or complicated membrane structures (Factor C); the number of intact clusters of peroxisomes from which GFP-SKL had not leaked out (Factor D); and the number of peroxisome clusters from which GFP-SKL fluorescence had diffused into the

---

1. *Abbreviations used in this paper*: ABTS, 2,2′-azino-bis(3-ethylbenzthiazoline-6-sulfonic acid); AOX, alcohol oxidase; DHAS, dihydroxyacetone synthase; FM4-64, *N*-(3-triethylammoniumpropyl)-4-(*p*-diethylaminophenylhexatrienyl) pyridinium dibromide; GFP, green fluorescent protein (S65T mutant version); G6PDH, glucose-6-phosphate dehydrogenase; NTG, 1-methyl-3-nitro-1-nitrosoguanidine; PEX, peroxin; PI3-kinase, phosphoinositide 3-kinase; PTS, peroxisomal targeting signal; SD, synthetic/dextrose; SM, synthetic/methanol; SE, synthetic/ethanol; SKL, serine-lysine-leucine; YPD, yeast extract/peptone/dextrose; YND, yeast nitrogen-base/dextrose; YNM, yeast nitrogen-base/methanol.

vacuolar matrix (Factor E). Factors A, B, and C, representing the FM4-64–stained vacuolar membrane, were counted using the rhodamine channel; and Factors D and E were counted using the fluorescein channel for GFP-SKL. Morphological changes of vacuoles were expressed as follows: stage 0 cells [(Factor A × 100)/Factors (A + B + C)]; stage 1 cells [(Factor B × 100)/Factors (A + B + C)]; stage 2 + 3 cells [(Factor C × 100)/Factors (A + B + C)]; and the percentage of peroxisome clusters degraded in the vacuole was given by [(Factor D × 100)/Factors (D + E)].

We recently reported that GFP fluorescence leaks through the rhodamine channel after excitation in the FITC channel (Sakai and Subramani, 1997). Therefore, samples were always observed first in the rhodamine channel to count the percentage of cells having the specified vacuolar morphology (Factors A, B, and C), and then peroxisome morphology (Factors D and E) was determined using the FITC channel. At least 300–400 total vacuoles and peroxisome clusters were counted in random fields at each time point. Fluorescence images were acquired using a CCD camera (model 4995; COHU, San Diego, CA) and a CG-7 Frame Grabber (Scion Corp., Frederick, MD). The software used was NIH Image 1.55 and Adobe Photoshop 3.0.

Electron Microscopy

Cells were fixed with 2% paraformaldehyde/0.5% glutaraldehyde for 1 h on ice, washed well with double-distilled water, resuspended in 1.5% potassium permanganate, incubated for 20 min at room temperature, washed with water, resuspended in 2% uranyl acetate, and spun for 15 min in an Eppendorf microcentrifuge. After additional washing the cells were dehydrated through a graded series of ethanol, transferred into propylene oxide, and embedded in Eponate 12 (Pelco International, Redding, CA). Thin sections were cut on a Reichert-Jung Ultracut E ultramicrotome (Leica Co., Deerfield, IL), stained with uranyl acetate and lead citrate, and examined in a Philips CM12 TEM. Micrographs were taken with a Gatan Retractable Multiscan CCD camera (Gatan Co., Pleasanton, CA).

Mutant Isolation and Visualization of Alcohol Oxidase Activity In Situ

Isolation of *pag* mutants was performed as follows: strain STW3 was mutagenized with NTG (Gould et al., 1992). Mutagenized cells were plated on glucose plates (∼600 cells/plate) and colonies were replica plated onto a nylon membrane filter that had been placed on a SM plate. The plates were incubated at 30°C for 2 d during which time the peroxisomal enzyme, alcohol oxidase, was induced. The filters were then transferred to a SD plate to induce microautophagic degradation of peroxisomes and, thereby, the degradation of alcohol oxidase. After 8 h on glucose plates, colonies on the filters were visualized for alcohol oxidase activity in situ. For this purpose, colonies on the filters were frozen in liquid nitrogen, thawed, and placed on a Whatman paper wetted in the alcohol oxidase assay mixture containing 6 mM ABTS, 20 U/ml peroxidase, 100 mM methanol in 50 mM potassium phosphate buffer, pH 7.0. Green- or purple-colored colonies showing alcohol oxidase activity after this glucose-shift were picked up from the master plate and subjected to a second and third screening. Mutants were backcrossed against the wild-type strain and placed into complementation groups.

Western Blot and Protein Analysis

Cultures of logarithmically grown PPY12 or mutant strain *pag4* in YNM were washed and resuspended in yeast nitrogen-base/dextrose (YND) at an OD_{600} of 0.1. Cells (40 OD units) were collected at each time point (0, 4, and 8 h), pelleted by centrifugation at 2,000 *g*, and resuspended in 400 μl potassium phosphate, pH 7.4, with protease inhibitors (1 mM PMSF in ethanol, 12.5 μg/ml leupeptin, 5 μg/ml aprotinin and 5 mM NaF). Glass beads (100 μl) were added and the mixture was vortexed for 10 min. After centrifugation for 3 min at 2,000 *g*, the protein concentration of the supernatant was determined and protein samples (10 μg) for each time point were analyzed by SDS-PAGE and Western blotting.

Results

Vital Staining of P. pastoris Vacuolar Membranes with FM4-64 and Peroxisomes with GFP-SKL

We have shown earlier that the fusion of the PTS1 pep-

tide, SKL, to the COOH terminus of GFP targets the latter to the peroxisomal matrix and that this fusion protein can be exploited as a vital stain for the peroxisomes (Monosov et al., 1996). To study autophagic degradation of peroxisomes in vivo, methanol-grown *P. pastoris* wild-type cells (strain STW1, expressing GFP-SKL) were labeled with FM4-64 (Vida and Emr, 1995). During endocytosis, FM4-64 stained punctate endosomes that did not overlap with the GFP-labeled peroxisomes (data not shown). Once in the vacuolar membrane, FM4-64 was stable for at least 8 h in cells grown on methanol, ethanol, or glucose media. However, FM4-64 in the vacuolar membrane diffused into the vacuolar matrix when cells were transferred to oleate or glycerol media (data not shown). Cells labeled with the two fluorescent markers, GFP-SKL and FM4-64, grew normally at doubling times similar to those exhibited by wild-type cells, suggesting that the labeling procedures did not adversely affect cell viability or the autophagic process under study.

Morphological and Kinetic Analyses of Intermediates in Microautophagy of Peroxisomes in Wild-type P. pastoris Cells

The cells labeled with the two markers were transferred
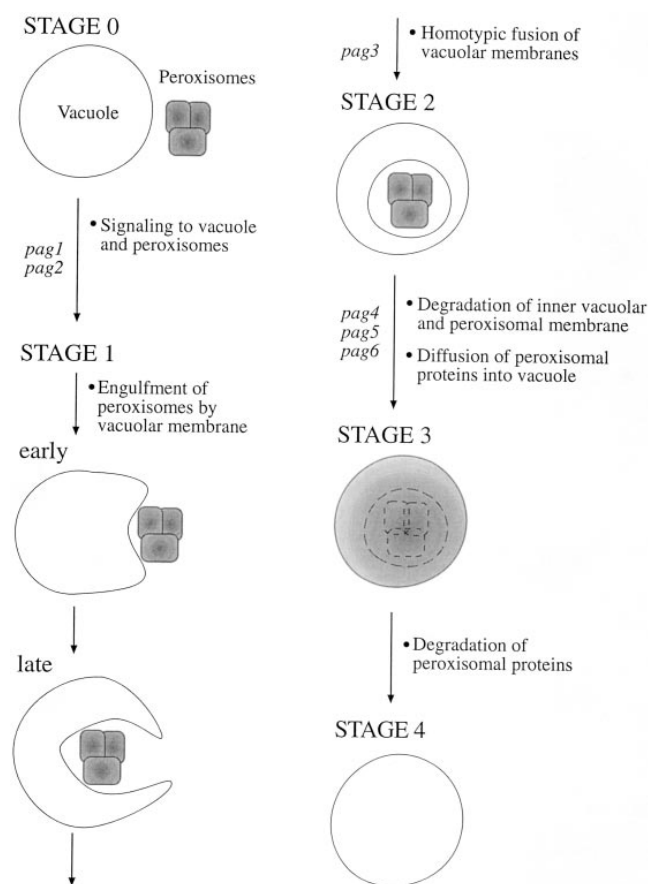

Figure 1. Schematic model of microautophagic degradation of peroxisomes in *P. pastoris*. Microautophagic degradation of peroxisomes is dissected into four stages (see text) depending on the morphology and the appearance and disappearance of intermediates in the process. Mutations in specific *PAG* genes terminate this process at the stages indicated.
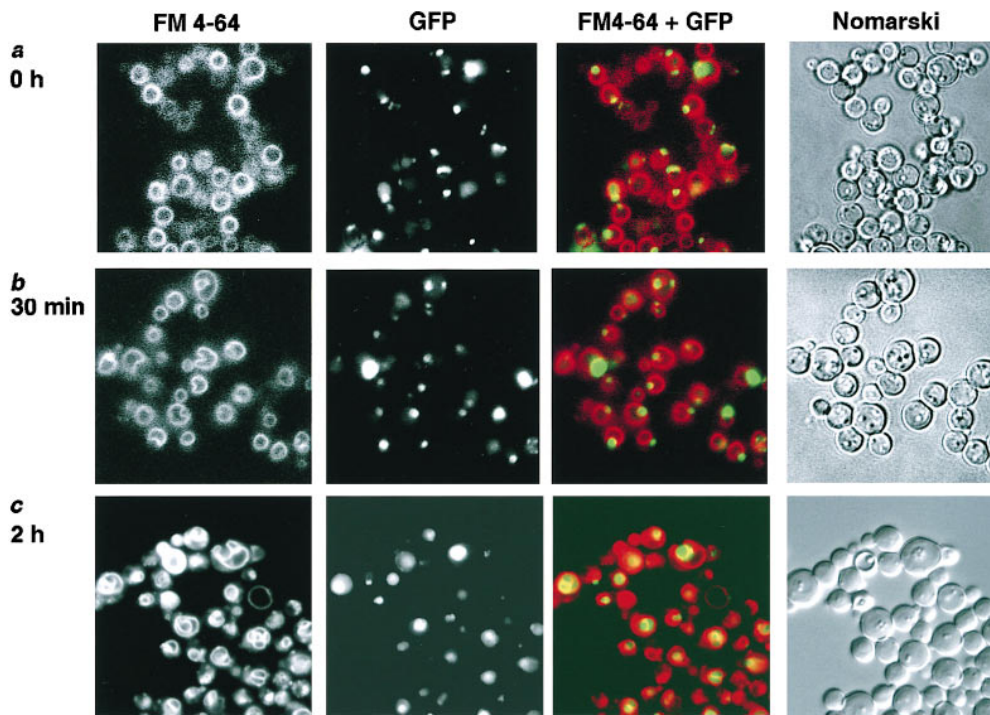
Figure 2. Morphological changes of vacuolar membranes and peroxisomal GFP-SKL during microautophagic degradation of peroxisomes after glucose adaptation. Double fluorescence of methanol-grown cells of *P. pastoris* cells at various times after the switch to glucose medium. (*a*) 0 h, (*b*) 30 min, (*c*) 2 h.

from methanol medium (which induces peroxisomes) to glucose medium (where the excess peroxisomes are degraded by microautophagy) and examined by fluorescence microscopy. A variety of morphological steps could be distinguished that are represented schematically as stage 0, early stage 1, late stage 1, and stages 2–4 (Fig. 1). Before transfer to glucose medium (Fig. 1, stage 0), most methanol grown cells contained one very large spherical vacuole per cell and a cluster of methanol-induced peroxisomes (Figs. 1 and 2 *a*). Although the vacuole and the peroxisomes were close to each other, most vacuoles (>90% in the cell population) did not show any invagination of their FM4-64–labeled membranes, and GFP-SKL exhibited a punctate fluorescence pattern characteristic of peroxisomes (Figs. 1 and 2 *a*). After 30 min in glucose medium, more than half the vacuoles were either slightly (Fig. 1, early stage 1) or deeply (Fig. 1, late stage 1) invaginated with a cluster of intact peroxisomes at the point of invagination (Figs. 1 and 2 *b*). After 2 h, the vacuolar membrane and peroxisomes showed a more complex morphology (Fig. 2 *c*) in which many of the vacuoles showed double- or multiple-membrane structures containing a cluster of peroxisomes (Fig. 1, stages 2 and 3 and Fig. 2 *c*).

These different stages of microautophagic degradation of peroxisomes were more easily observed at higher magnification by both fluorescence (Fig. 3, *a–e*) and electron microscopy (Fig. 3, *f–i*). Stage 0 cells are shown in Fig. 3, *a* and *f*, early stage 1 cells are in Fig. 3, *b* and *g*, and late stage 1 cells are shown in Fig. 3, *c* and *h*. In stage 2 cells, the peroxisomes surrounded by the vacuolar membrane still remained intact, as the GFP-SKL had not yet leaked into the vacuolar matrix (Fig. 3, *d* and *i*). In contrast, in stage 3 cells, the GFP-SKL fluorescence had leaked into the vacuolar matrix (Fig. 3 *e*). Thus, we are able to detect the disintegration of peroxisomes not by monitoring per-

oxisomal protein degradation but by the leakage of GFP-SKL into the vacuolar matrix, and to define the stage (stage 3) at which peroxisome degradation began even though most of the peroxisomes appeared intact.

Then we applied morphometric analysis to determine the kinetics of the early stages. Fig. 4 shows the kinetics of transport and degradation of peroxisomes by microautophagy. After 30 min in glucose medium, the number of spherical vacuoles (stage 0) decreased drastically from ~85% to ~30%, and this was correlated with an increase to ~60% of stage 1 cells. At this time point, the number of vacuoles showing GFP-SKL diffusion into the vacuolar matrix remained at a basal level of under 10% (Fig. 4, stage 3). As the percentage of stage 1 cells decreased from 60% at 30 min down to ~20% at 180 min, vacuoles having double or complex membranes (stages 2 and 3) gradually increased and reached ~30% of the total number of vacuoles. The GFP-SKL release into the vacuolar matrix began to increase after a lag time of 60 min, which corresponds well with the time taken for the accumulation of stage 2 and stage 3 structures. After 3 h, about half of the peroxisomal clusters released their GFP-SKL into the vacuolar matrix. This kinetic analysis strongly suggests that the morphological changes of the vacuole (i.e., stages 0, 1, 2, 3, and 4) represent distinct steps of the autophagic process, and that stages 0 to 3 represent the early stages of microautophagy before the degradation of peroxisomal proteins by vacuolar proteases occurs (stage 4).

Vacuoles with Double or Complicated Membrane Structures Are Not Detected During Macroautophagy

A similar analysis was performed for the degradation of peroxisomes via macroautophagy by transferring *P. pastoris* wild-type cells from methanol to ethanol medium.
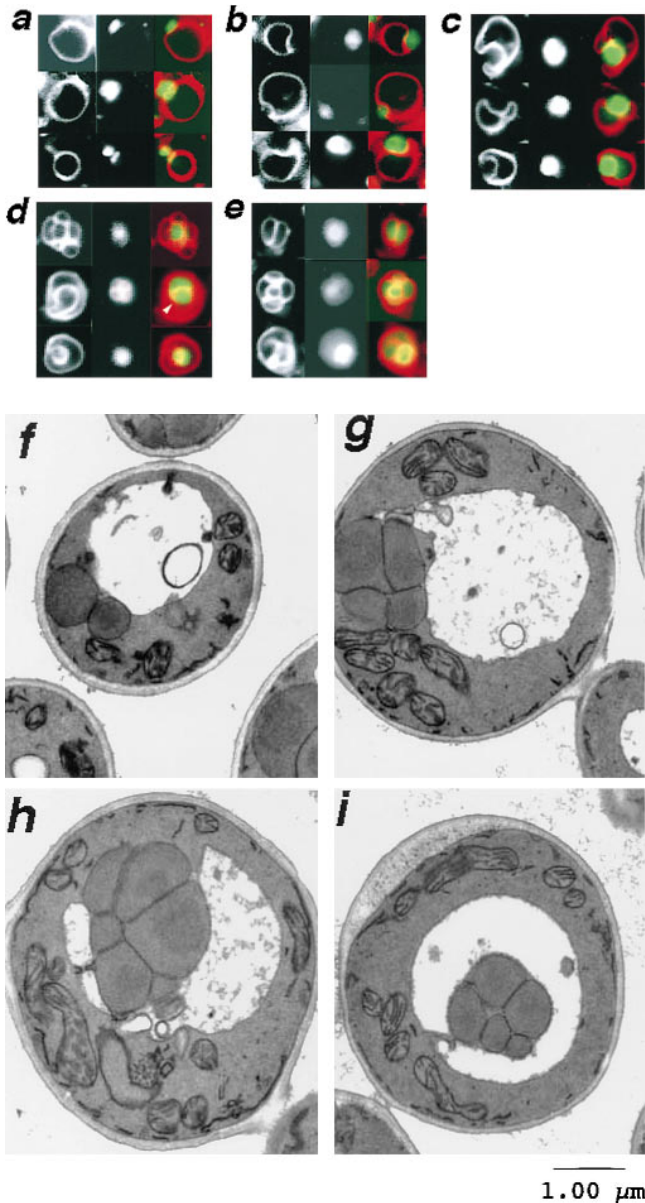
Figure 3. Fluorescence and electron microscope images showing various stages during microautophagic degradation of peroxisomes. The three panels in each figure are as follows (*a–e, left*) FM4-64; (*center*) GFP-SKL; (*right*) superimposed FM4-64 and GFP-SKL signals. (*a, f*) stage 0; (*b, g*) early stage 1; (*c, h*) late stage 1; (*d, i*) stage 2; (*e*) stage 3. (*d, arrowhead*) During the capture of these fluorescence images, this peroxisome-containing vesicle had just pinched off from the outer vacuolar membrane. Therefore, the FM4-64–stained vesicle membrane and GFP-SKL could not be superimposed in this picture.

After 1 h of ethanol adaptation, peroxisomes were surrounded by membranes (Fig. 5, *a, d,* and *e*) that were at times juxtaposed adjacent to the nuclear envelope (Fig. 5 *d*). Between 0–60 min when the spherical vacuoles were decreasing (Fig. 5 *f, Stage 0*), the percentage of invaginated vacuoles (Fig. 5 *f, Stage 1*) reached a value of ~40% after 30 min, but the formation of multiple vacuolar membranes (Fig. 5 *f, Stage 2 + Stage 3*) was not observed. However, peroxisomal GFP-SKL was delivered to the vacuolar ma-

trix and showed more rapid kinetics than the microautophagic degradation of peroxisomes. No lag was observed in the degradation of GFP-SKL by the macroautophagic pathway (Fig. 5 *f, Stage 3*). The vacuoles invaginated slightly where peroxisomes contacted them (Fig. 5 *b*), but they already showed the release of GFP-SKL in the vacuolar matrix (Fig. 5 *g*). These observations are consistent with the fusion of the vacuolar membrane with the autophagosomal membranes that surround the peroxisomes. At this stage, peroxisomes come in contact with the vacuolar matrix, the integrity of the peroxisomal membranes is lost, and GFP-SKL leaks into the vacuolar matrix (Fig. 5 *b*). In addition, autophagic bodies were also observed inside the vacuole (Fig. 5 *c*).

Inhibitors Affect Macroautophagy and Microautophagy Differentially

Since we were in a position to observe the early stages of microautophagy of peroxisomes, several reagents were tested to (*a*) investigate the stage at which they block the process in vivo, and (*b*) to see if they affected both autophagic pathways simultaneously.

Cycloheximide. As the degradation of peroxisomal proteins is inhibited by cycloheximide in glucose adaptation but not in ethanol adaptation (Tuttle and Dunn, 1995), *P. pastoris* cells were transferred from methanol to ethanol and glucose media with and without cycloheximide (1 mg/ml). Under these conditions, protein synthesis of *P. pastoris* is inhibited ~90% (Tuttle and Dunn, 1995). Although the addition of the drug during ethanol adaptation did not inhibit the rate of peroxisome degradation detected by GFP-SKL diffusion into the vacuolar matrix, its addition during glucose adaptation did inhibit the degradation of GFP-SKL by microautophagy (Fig. 6, *a* and *b, Stage 3*). Looking at the kinetic data, slight invagination of vacuoles by peroxisomes was not inhibited (Fig. 6 *a, Stage 1*), but no vacuole showed any deep invagination or formation of double or complex vacuolar membrane structures (Fig. 6 *a, Stage 2 + Stage 3*). Therefore, cycloheximide inhibits the step between early and late stage 1, suggesting that newly synthesized proteins are necessary for later stages of microautophagy.

PMSF and Protease-negative Mutants. The protease inhibitor PMSF inhibits macroautophagy and the vacuolar proteases such as proteinase B are required for macroautophagy in *S. cerevisiae* but the step that is inhibited is unknown (Takeshige et al., 1992). Wild-type *P. pastoris* cells were treated with PMSF (3 mM). During ethanol adaptation, PMSF did not inhibit the transport of peroxisomes to, or the release of GFP-SKL into, the vacuolar matrix (Fig. 6 *b, Stage 3*). The absence of degradation of the GFP-SKL released into the vacuole (data not shown) defines the requirement for vacuolar proteases for this last degradative step of macroautophagy. During glucose adaptation, some GFP-SKL diffused into the vacuolar matrix (Fig. 6 *a, Stage 3*). However, during the degradation, the percentage of stage 1 structures formed was greatly diminished relative to that seen in the absence of PMSF (Fig. 6 *a, Stage 1*). Furthermore, we did not find double or complex vacuolar membranes (Fig. 6 *a, Stage 2 + Stage 3*). It is quite possible that when microautophagy is inhibited, low levels of mac-

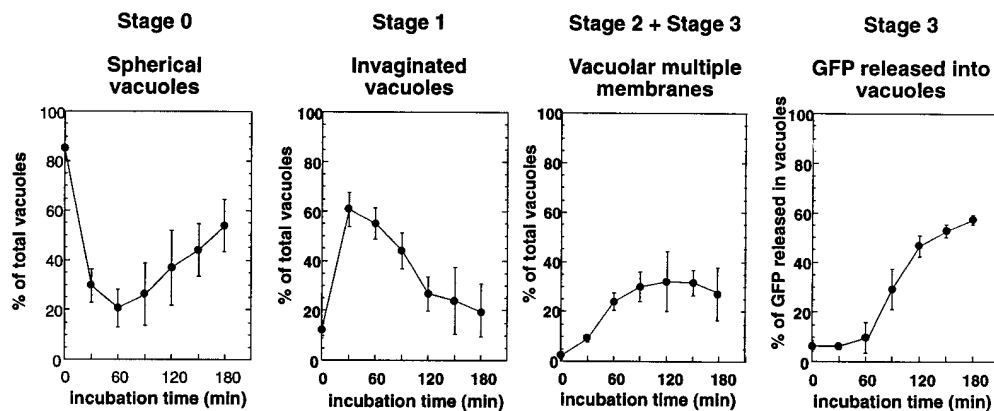Stage 0 | Stage 1 | Stage 2 + Stage 3 | Stage 3

Figure 4. Kinetics of morphological changes in vacuoles and peroxisomal GFP-SKL during microautophagic degradation of *P. pastoris* peroxisomes in glucose adaptation. At least 350 vacuoles or 350 clusters of peroxisomes were counted for each time point. Cells were counted in three randomly selected fields, and standard deviations are shown as vertical bars.

roautophagy may account for the residual release of GFP-SKL into the vacuoles during glucose adaptation. Indirect evidence in support of this possibility has also been provided by Yuan et al. (1997).

Next, we investigated these autophagic processes using the protease-negative strain STK7, in which vacuolar proteinases A and B are inactivated (Fig. 7, *a–c*). Similar to PMSF-treated cells, this mutant failed to accumulate high levels of the stage 1 structures (Fig. 7 *a*) and did not show any formation of double or complex vacuolar membranes during glucose adaptation (Fig. 7 *a*, *Stage 2 + Stage 3*). The percentage of invaginated vacuoles remained low (10–20%) after the shift to glucose medium (Fig. 7 *a*, early stage 1 cells). However, small amounts of GFP-SKL were still delivered to the vacuolar matrix but at a rate slower than in wild-type cells (Fig. 7 *a, Stage 3*). In ethanol adaptation, however, the rate of GFP-SKL delivery to the vacuolar matrix of STK7 was comparable to that of the wild-type strain (Fig. 7 *b, Stage 3*).

These results suggest that the activity of vacuolar proteases is necessary for delivery of peroxisomes to the vacuole via the microautophagic process between stage 0 and stage 1, i.e., the invagination process of the vacuole. In contrast, the delivery of peroxisomes to the vacuole via macroautophagy is not inhibited in protease-negative or PMSF-treated cells.

Wortmannin. Wortmannin is a specific inhibitor of PI3-kinase (Stack and Emr, 1994) and has been reported to inhibit autophagy in hepatocytes (Blommaart et al., 1997). Wortmannin (1 mM) inhibited the formation of double and complex vacuolar membranes in microautophagy but did not inhibit transport of peroxisomes to the vacuole by macroautophagy (Fig. 6, *a* and *b*). One of the differences between wortmannin- and PMSF-treated cells is that wortmannin inhibited all invagination of the vacuole and wortmannin-treated cells showed very spherical vacuoles. Before adaptation in glucose or ethanol media, ~10% of the cells showed a slight invagination of the vacuole by peroxisomes. Although treatment by PMSF did not change the basal level of invagination after 30 min, treatment by wortmannin seemed to block microautophagic degradation of peroxisomes between stage 0 and stage 1. However, as with PMSF, when microautophagy was inhibited by wortmannin during glucose adaptation, some release of GFP-SKL into the vacuole did occur, perhaps by macroautophagy (Fig. 6 *a*).

Genetic Dissection of the Microautophagic Degradation of Peroxisomes

P. pastoris cells (STW3) were mutagenized and *pag* mutants (deficient in peroxisome degradation via autophagy) were isolated. We classified these recessive *pag* mutants into six complementation groups (*pag1* to *pag 6*). The *pag* mutants showed alcohol oxidase activity after glucose adaptation, while the wild-type strain did not (Fig. 8 *a*). Whereas the wild-type PPY12 strain did not show any alcohol oxidase after 8 h of glucose adaptation, the *pag4* strain still contained a significant amount of this protein (Fig. 8 *b*). Western blots with the mitochondrial F1β subunit and the cytosolic glucose-6-phosphate dehydrogenase (G6PDH) indicated that the degradation was specific for alcohol oxidase, and therefore the peroxisome. The growth curve revealed that the two strains grew at similar rates and that the stability of alcohol oxidase was not due to slower growth of the *pag4* strain (Fig. 8 *b*). The level of the alcohol oxidase in the *pag4* strain after 8 h of glucose adaptation was less than at 0 h because the strain grows in glucose but does not produce any alcohol oxidase under glucose-repressed conditions.

Classification of pag Mutants by Morphological Analysis

We characterized the morphological phenotypes of these mutants further during the microautophagic degradation of peroxisomes.

Mutants Blocked between Stage 0 and Stage 1 (pag1 and pag2). During glucose adaptation, the *pag1* mutant showed neither invagination of the vacuole, nor formation of vacuolar double-membrane structures, nor release of GFP-SKL into the vacuolar matrix (data not shown). Thus, vacuoles of a *pag1* mutant showed no response to the shift from methanol to glucose medium, and remained spherical. This mutant may be impaired in a very early stage of microautophagy, possibly in the signal-transduction pathway that is activated upon shift to glucose, or in the response of the vacuolar membrane to such a signal.

Another mutant belonging to this group, *pag2*, is characterized by its abnormal vacuolar morphology that was unaffected by the growth media, i.e., methanol, ethanol, or glucose medium (Fig. 9 *a*). GFP-SKL release into the vacuolar matrix was not observed after glucose adaptation and peroxisomes remained intact after glucose adaptation.
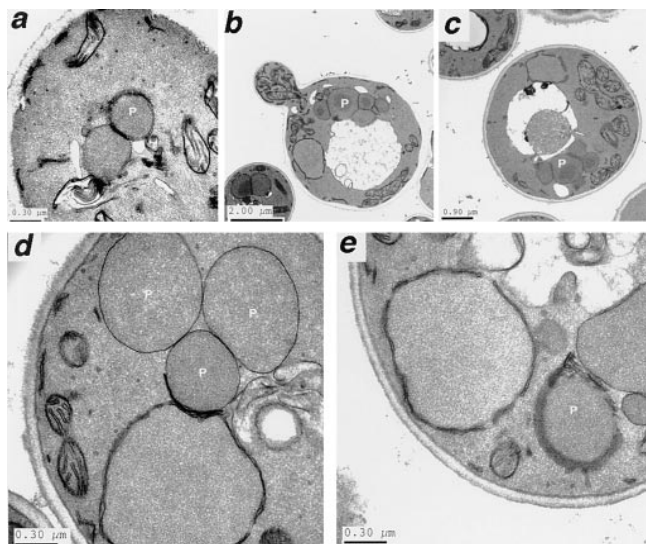
Figure 5. Macroautophagic degradation of peroxisomes after transfer of methanol-grown *P. pastoris* cells to ethanol medium. (*a–e*) Electron micrographs of intermediates seen during macroautophagy. (*a*) After 1 h of ethanol adaptation, peroxisomes (P) were often surrounded by autophagosomal membranes, higher magnifications of which are in *d* and *e*. (*b*) After 1 h of ethanol adaptation, the autophagosomal membrane surrounding the peroxisomes appears to have fused with the vacuolar membrane. (*c*) At 2 h a peroxisome in the form of an autophagic body is seen within the vacuole. Magnified pictures of samples obtained at the (*d*) 20 min time point showing the nuclear endoplasmic reticulum membrane in close proximity to the membranes surrounding the peroxisomes, and at the (*e*) 1 h time point demonstrating peroxisomes surrounded by multiple autophagosomal membranes. (*f*) Kinetics of morphological changes in vacuoles and peroxisomal GFP-SKL. Other conditions are described in *Materials and Methods*, and are the same as in Fig. 4. (*g*) Fluorescence images taken after 2 h of ethanol adaptation of wild-type *P. pastoris* cells.
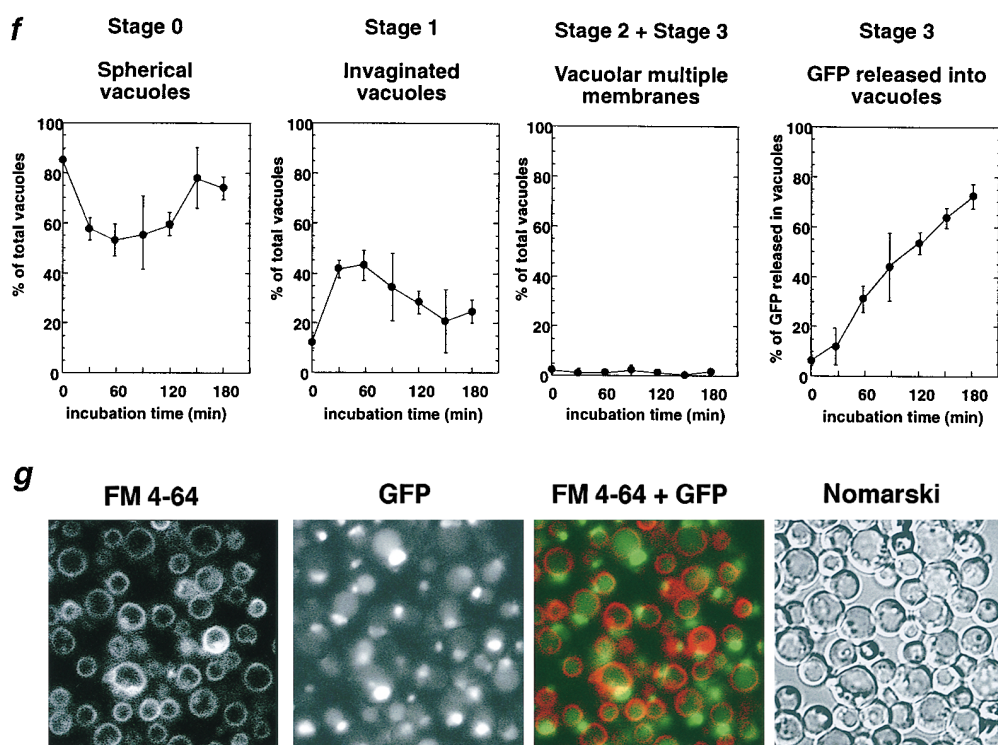
We believe that the *pag2* mutant is defective in its ability to engulf peroxisomes properly for microautophagy.

Mutants Blocked between Stage 1 and Stage 2 (pag3). The *pag3* mutation is characterized by its deeply invaginated structure of the vacuole after 2.5 h of glucose adaptation (Fig. 9 *b*). However, we were unable to find vacuoles having double or complex membrane structures or diffusion of GFP-SKL in the vacuole matrix even after longer incubation periods. We classify the *pag3* mutant as one that is blocked between late stage 1 and stage 2 in the model shown in Fig. 1.

Mutants Blocked between Stage 2 and Stage 3 (pag4, pag5, and pag6). The *pag4* mutant showed a unique vacuolar membrane morphology (Fig. 10). Before glucose adaptation, most vacuoles were spherical or slightly invaginated with peroxisomes (Fig. 10 *a*). During glucose adaptation,

the *pag4* strain formed double or complicated vacuolar membrane structures surrounding peroxisomes (Fig. 10 *b*) and was characterized by continued proliferation of the vacuolar membrane surrounding the peroxisomes for at least 6–8 h. However, GFP-SKL diffusion into the vacuolar matrix was never found, indicating that peroxisomes were still intact within the vacuole. Even as the vacuolar membrane became more complex, GFP-SKL did not diffuse into the vacuolar matrix (Fig. 10 *c*). It seems that the *pag4* mutant is impaired in proper control of vacuolar membrane proliferation or in the release of GFP-SKL into the vacuole.

The *pag5* and *pag6* mutants displayed similar phenotypes during microautophagy. In both mutants, microautophagic degradation of peroxisomes proceeded normally until double or complex vacuolar membrane formation as

a Glucose-adaptation
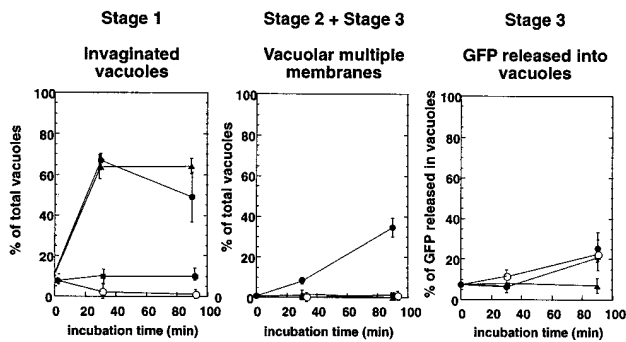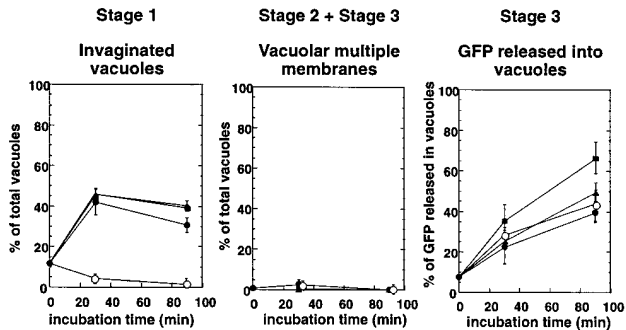

b Ethanol-adaptation

Figure 6. Effect of inhibitors on transport of peroxisomal GFP-SKL to, and degradation in, vacuoles during (*a*) glucose adaptation and (*b*) ethanol adaptation. Wortmannin and PMSF were dissolved in DMSO, and added to the glucose medium. (*Filled circle*) Control (2% DMSO); (*open circle*) 1 mM wortmannin (with 2% DMSO); (*filled square*) 3 mM PMSF (with 2% DMSO); (*filled triangle*) 10 mg/ml cycloheximide.

described in the wild-type strain, but GFP-SKL was not released into the vacuolar matrix. In *pag5* and *pag6* mutants, however, we did not observe extensive vacuolar membrane proliferation as observed in the *pag4* mutant. From these results, we categorize the *pag4*, *pag5*, and *pag6* mutants into the group where microautophagic degradation of peroxisomes is blocked between stages 2 and 3.
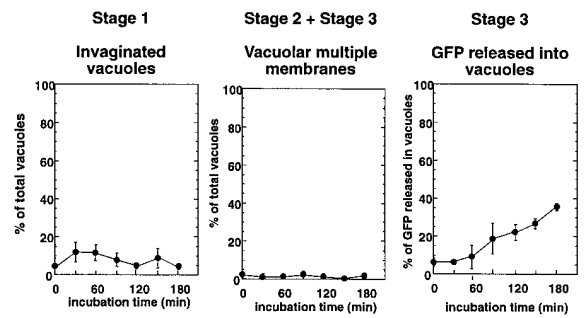
Peroxisome Degradation after Ethanol Adaptation Is Inhibited in pag4 and pag5, but Not in Other, pag Mutants

In ethanol adaptation of *pag1*, *pag2*, *pag3*, *pag6* strains, peroxisomes were delivered to the vacuole, and GFP-SKL diffusion into the vacuolar matrix was observed, as seen for the wild-type strain. In contrast, both *pag4* and *pag5* mutant strains did not show any GFP-SKL diffusion into the vacuolar matrix. The alcohol oxidase activity assay also showed that *pag4* and *pag5* mutants were unable to degrade alcohol oxidase during ethanol adaptation (Fig. 8 *a*). Thus there is at least a partial convergence of the machinery (e.g., Pag4p and Pag5p) in both microautophagic and macroautophagic degradation of peroxisomes.
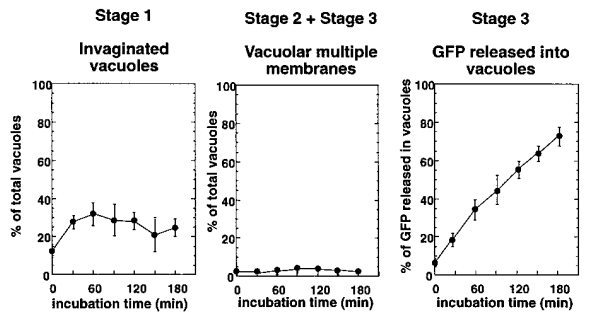
Peroxisome Assembly and Degradation by Microautophagy Are Independent Processes

A *P. pastoris pex1-ts* strain expressing GFP-SKL was

a Glucose-adaptation (STK7)

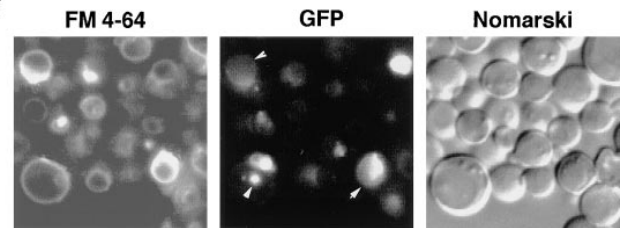**b Ethanol-adaptation (STK7)**

c

Figure 7. Microautophagic degradation of peroxisomes is not observed in a vacuolar protease-negative strain (STK7) of *P. pastoris*. Kinetics of morphological changes in vacuoles and peroxisomal GFP-SKL during (*a*) glucose adaptation and (*b*) ethanol adaptation. (*c*) Fluorescence images taken after 2 h of glucose adaptation. Arrows show GFP-SKL in vacuolar matrix. Some cells showed diffusion of GFP-SKL into the vacuolar matrix.

grown in methanol medium at the permissive temperature (22°C), and transferred to glucose medium at 22 and 34°C. The transport of peroxisomes to the vacuole via the normal microautophagic processes was slower at the restrictive temperature (34°C) than at the permissive (22°C; Fig. 11 *a*). Since the *pex1-ts* mutant is not able to assemble normal peroxisomes at 34°C, peroxisome assembly and microautophagy are not coupled processes.

Next, *pex1-ts* strain was grown on methanol at 34°C and then transferred to glucose medium where vacuolar morphology was observed. Before the transfer, the vacuole was spherical and morphologically similar to vacuoles of methanol-grown wild-type cells, and GFP-SKL was distributed diffusely in the cytosol but not in the vacuole (Fig. 11 *b*, 0 h). After transfer to glucose medium for 2 h, the vacuoles (~20–30%) showed complicated membrane structures (Fig. 8 *b*, 2 h). The same results were obtained using another peroxisome assembly mutant, *pex3*, which lacks detectable peroxisomes and peroxisome remnants. These
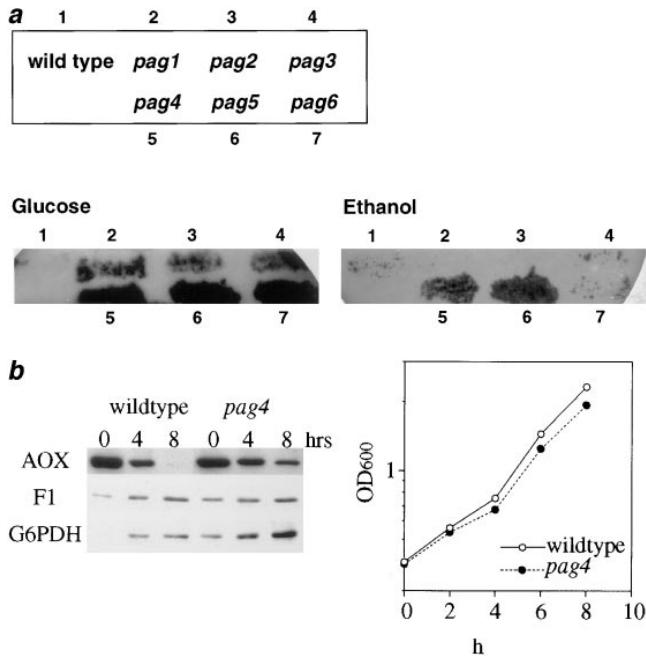
Figure 8. (*a*) Visualization of alcohol oxidase activity in colonies after (*a*) glucose adaptation for 8 h and ethanol adaptation for 24 h in wild-type (strain PPY12) and *pag* mutant cells (strains STK1-STK6, *Materials and Methods*) of *P. pastoris*. (*b*) Western-blot analysis of samples taken from cultures shifted from methanol to glucose for the indicated time. Antibodies used were *AOX*, alcohol oxidase; *F1*, mitochondrial F1β subunit; *G6PDH*, glucose-6-phosphate dehydrogenase. Growth curve of the wild-type strain PPY12 and the *pag4* mutant (strain STK4) after shift from methanol to glucose.

results suggest that the vacuole responds to the signal for microautophagy even when normal peroxisomes are absent from the cell.

Discussion

P. pastoris as a Model System for Studies on Autophagy

The ability to mark efficiently and specifically peroxisomes with the fusion protein GFP-SKL and the vacuole

membrane with FM4-64 has enabled us to monitor the morphological and kinetic changes involved in two types of autophagic processes (Tuttle and Dunn, 1995). *P. pastoris* offers significant advantages over *S. cerevisiae* (Tsukada and Ohsumi, 1993; Thumm et al., 1994; Noda et al., 1995; Harding et al., 1996) or *H. polymorpha* (Titorenko et al., 1995), as either macroautophagy or microautophagy of peroxisomes can be activated by specific nutritional cues. Upon shift of cells from peroxisome-inducing medium (e.g., methanol) to ethanol or glucose, the excess peroxisomes are degraded by macro- or microautophagy, respectively. The analysis of these two processes in the same organism permits an evaluation, both genetically and biochemically, of the extent of overlap between the two autophagic pathways.

Distinct Morphological and Kinetic Intermediates Are Detectable During Microautophagy in P. pastoris

Although the autophagic processes in *P. pastoris* have been characterized in some detail and a few mutants deficient in this process have been isolated (Tuttle and Dunn, 1995), our knowledge of the morphological and kinetic intermediates involved is still rudimentary. In previous studies, peroxisome degradation was studied by monitoring protein degradation (e.g., alcohol oxidase). However, since protein degradation occurs only at the very last stage of autophagy, it was not possible to follow the early stages of peroxisome degradation by following protein turnover. Additionally, a kinetic analysis of the intermediates is essential for an understanding of the early stages of autophagy.

During the switch of *P. pastoris* cells from methanol to glucose medium, a series of distinct morphological intermediates could be distinguished, and confirmed by electron microscopy, in particular at the earliest stages of microautophagy. Just before the activation of microautophagy, most methanol-grown cells have one large, spherical vacuole per cell (Figs. 1 and 2 *a*). Within a few minutes (5–10 min) after the shift to glucose, the cells respond by invagination of the vacuolar membranes (Fig. 1, early stage 1 and Fig. 4, *Stage 1*). The appearance of these vacuoles with slight (Fig. 1, early stage 1 and Fig. 3, *b* and *g*) or deep invaginations (Fig. 1, late stage 1 and Fig. 3, *c* and *h*) of the vacuolar membranes is accompanied by the concomitant
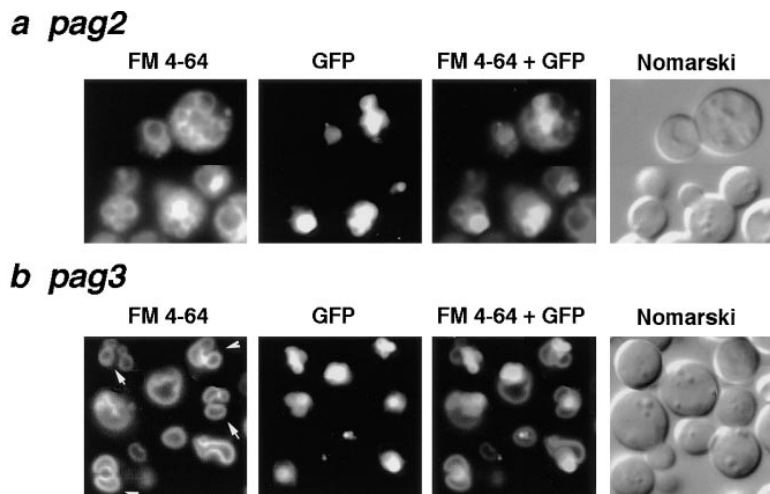

Figure 9. Fluorescence images of (*a*) *pag2* (strain STK2) and (*b*) *pag3* (strain STK3) mutants of *P. pastoris* after a 3 h shift to glucose. (*b*) Arrows show deeply invaginated structures of vacuolar membranes surrounding peroxisomes in the *pag3* mutant.
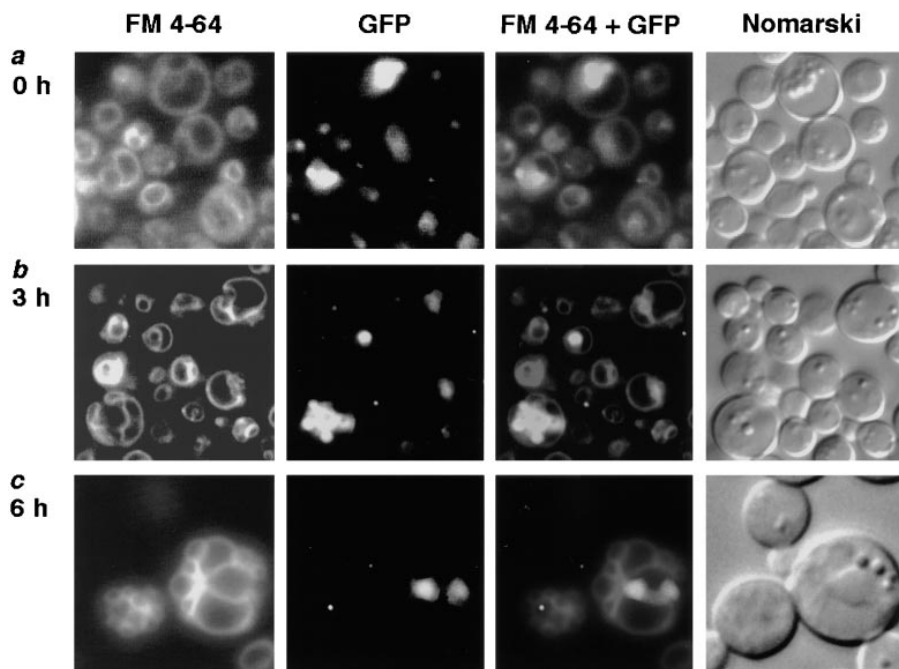
| FM 4-64 | GFP | FM 4-64 + GFP | Nomarski |

a 0 h

b 3 h

c 6 h

Figure 10. Fluorescence images of the *pag4* (strain STK4) mutant of *P. pastoris* after (*a*) 0, (*b*) 3, or (*c*) 6 h of glucose adaptation. The vacuolar membrane proliferated extensively and surrounded peroxisomes during glucose adaptation.

disappearance of the spherical vacuoles (Fig. 1, stage 0 and Fig. 2 *a*), reminiscent of a precursor–product relationship between the two types of structures (Fig. 4). There was often a cluster of peroxisomes in close association with the invaginated vacuolar membrane, raising the question as to whether the peroxisomes were responsible for the alteration of the vacuolar membrane. This is unlikely since similar changes of the morphology of the vacuolar membrane were observed in a mutant deficient in peroxisome assembly (Fig. 11, *pex1-ts*), as well as in the *pex3* mutant that lacks peroxisomal remnants (Wiemer et al., 1996).

After the invagination of the vacuolar membrane around the peroxisomes (or peroxisome clusters) the vacuolar membrane appeared to completely engulf the peroxisomes, so that a double membrane formed around the peroxisomes. The outer of these two membranes is derived from the vacuolar membrane (Fig. 1, *Stage 2*). These two-membrane structures might form by homotypic fusion of the vacuolar membrane that engulfs the peroxisomes. This is followed by the appearance of structures in which the peroxisomes are surrounded by more complex, and multiple, vacuolar membranes (Fig. 1, *Stage 3*). These membrane structures might arise by further homotypic fusion events involving the vacuolar membrane such that the vacuole subdivides into multiple compartments whose membranes are still labeled with FM4-64. A precursor–product relationship was observed between the stage 1 structures and the stage 2 and stage 3 structures (Fig. 4). It is only after the accumulation of these stage 2 and stage 3 structures reaches a maximum (at ∼60 min) that the release of GFP-SKL is detected into the vacuoles (Fig. 4). In stage 3, the structural integrity of the peroxisome membrane is compromised, and GFP-SKL leaks out to fill the vacuolar matrix. Finally, the vacuolar proteases degrade the GFP-SKL so that its fluorescence disappears (Fig. 1, *Stage 4*).

The results of these experiments confirm previous observations that the vacuole is indeed the site of peroxisome degradation and that peroxisome clusters are delivered to the vacuole (Veenhuis et al., 1983; Tuttle et al., 1993; Tuttle and Dunn, 1995; Chiang et al., 1996). The quantitation of the stages of the microautophagy demonstrates that there are a series of intermediates (stages 0–4) that appear and disappear in a manner consistent with their involvement as successive kinetic intermediates in a linear pathway (Fig. 1). These studies therefore provide a working model for the steps in microautophagy. As described later, the intermediates proposed in the model are fully supported by the identification of mutants blocked at various stages of this proposed pathway.

Macroautophagy Is Similar in P. pastoris and in Other Yeasts

Previous studies have described in detail the process of macroautophagy in *S. cerevisiae* (Baba et al., 1994, 1995) and in *H. polymorpha* (Veenhuis et al., 1983; Titorenko et al., 1995). Upon shift of *P. pastoris* from methanol to ethanol medium, a similar process can be documented in *P. pastoris* (Tuttle and Dunn, 1995). The peroxisomes in the cytoplasm are first surrounded by membranes (Fig. 5 *a, d,* and *e*). Although the membranes surrounding the peroxisome and the nuclear ER are closely apposed, we cannot distinguish whether the new membranes are derived from the nuclear envelope (Fig. 5 *d*). The resulting structures, the autophagosomes, then contact the vacuolar membranes (Fig. 5 *b*). The outer membrane of the autophagosome fuses with the vacuolar membrane, and the peroxisomal membrane comes in contact with the vacuolar matrix. As this is followed by the disruption of the integrity of the peroxisomal membrane that is in contact with the vacuolar matrix, GFP-SKL is released into the vacuole where it is eventually degraded (Fig. 5 *b*). The peroxisomes often leak their contents into the vacuolar matrix while remaining adjacent to, and in contact with, the vacuole. Autophagic bodies are also observed within the vacuole (Fig. 5
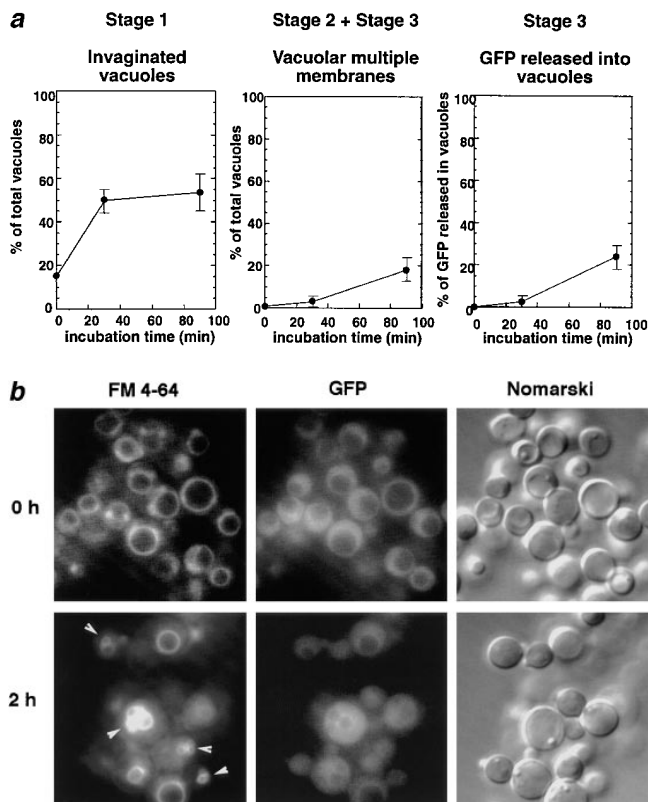
634

Figure 11. Microautophagy of peroxisomes in a *pex1-ts* mutant (strain SJH242) of *P. pastoris* expressing GFP-SKL from the constitutive glyceraldehyde-3-phosphate dehydrogenase (GAPDH) promoter at the restrictive temperature for peroxisome assembly (34°C). (*a*) Kinetics of peroxisome degradation at 34°C. Strain SJH242 was induced on methanol at 23°C, and glucose adaptation was performed at 34°C. (*b*) Changes in vacuole morphology were seen even in the absence of normal peroxisomes. At 0 h, SJH242 cells were grown at 34°C when GFP-SKL was diffuse in the cytosol and many vacuoles showed spherical morphologies. After 2 h, ~20–30% vacuoles showed complicated membrane structures representative of stage 2 cells.

c). Two features of macroautophagy that distinguish it from microautophagy are that the double and complex membrane structures seen during microautophagy are completely absent, and the release of GFP-SKL into the vacuole proceeds with a much shorter lag period, or none at all (Fig. 5 *f*).

Macroautophagy and Microautophagy Are Distinct Processes Affected Differentially by Inhibitors

The use of a variety of inhibitors known to affect autophagy in other organisms has helped to distinguish unique aspects of the two autophagic processes in *P. pastoris*. The protein synthesis inhibitor, cycloheximide, was reported earlier to affect micro-, but not macroautophagy (Tuttle and Dunn, 1995). However, the specific step affected by the cycloheximide treatment was not identified. Our morphological and kinetic analyses (Fig. 6, *a* and *b*) confirm the earlier reports (Tuttle and Dunn, 1995) and show that protein synthesis is required for the progression between early and late stage 1 of microautophagy.

PMSF inhibition of the major vacuolar proteinases A and B (Fig. 6, *a* and *b*) did not affect the delivery of peroxisomes to, or the release of GFP-SKL into, the vacuoles via macroautophagy but did inhibit the early stages of microautophagy. Similar results were confirmed in mutants deficient in the activities of these proteases (Fig. 7, *a* and *b*). These results are consistent with reports that, in *S. cerevisiae*, inhibition of vacuolar proteases causes the accumulation of autophagic bodies whose contents remain undegraded inside vacuoles (Takeshige et al., 1992). Interestingly, when microautophagy was inhibited, some release of GFP-SKL into the vacuole was still observed. We believe that this is not due to microautophagy because the intermediates characteristic of this process (stages 1–3) were either greatly diminished or absent. It is possible that the degradation of GFP-SKL under these conditions is due to a low level of macroautophagy or due to the activation of some other degradative pathway.

Although proteases A and B appear not to be required for the delivery of GFP-SKL to the vacuole via macroautophagy, these results also indicate that the activity of vacuolar proteases is required between stages 0 and 1 of the microautophagic process. The absence of vacuolar proteases would, of course, be expected to affect the final degradation of the GFP-SKL delivered to the vacuole by either autophagic process. The kinetic experiments presented here did not address this point because they did not follow the disappearance of GFP-SKL from the vacuole. Additionally, wortmannin also differentially affected microautophagy at its earliest stage (transition from stage 0 to stage 1) without significant effects on macroautophagy.

Collectively, these studies show that whereas microautophagy requires protein synthesis, as well as the activities of the vacuolar proteases and PI3-kinases either directly or indirectly, the delivery of peroxisomal proteins to the vacuole by macroautophagy does not.

Mutants Defective in Microautophagy Support the Model Proposed for this Process

Although the strategy used for the isolation of the *pag* mutants, deficient in microautophagy, is similar to the ones used previously in *P. pastoris* (Tuttle et al., 1993) and *H. polymorpha* (Titorenko et al., 1995), the ability to distinguish the morphological and kinetic steps in autophagy has allowed us to classify these mutants and to use them to lend additional support for the model we propose (Fig. 1). Based on this analysis, the *pag1* and *pag2* mutants are impaired in the transition from stage 0 to stage 1, a process that requires the peroxisomes and the vacuole to respond to glucose signaling. These mutants could therefore be affected either in the signal-transduction pathway that senses or responds to the levels of glucose in the environment as in the *gsa1* mutant of *P. pastoris* (Yuan et al., 1997). The *pag3* mutant is capable of proceeding to late stage 1, but fails to form the double- and complex-membrane structures that arise probably from homotypic fusion events involving the vacuolar membrane. The *pag4*, *pag5*, and *pag6* mutants are affected between stages 2 and 3, because they accumulate the complex-membrane structures surrounding the peroxisomes, but fail to release the GFP-SKL into the vacuolar matrix. None of the *pag* mu-

tants described appear to be deficient in the labeling of the vacuolar membrane by endocytosis, nor are they deficient in vacuolar inheritance (Figs. 9 and 10).

Although the mutants described in this study represent the results of a small-scale screen, their utility is already obvious in that they support several steps of the model (Fig. 1), and show that although some mutants (e.g., *pag1*, *pag2, pag3,* and *pag6* in Fig. 8 *a*) affected in microautophagy are normal for macroautophagy, others (e.g., *pag4* and *pag5* in Fig. 8 *a*) are compromised in both autophagic processes. This is to be expected since both pathways converge on the vacuole, where they are likely to share degradative steps. The morphometric and kinetic analyses described here will serve as powerful tools to characterize these and additional mutants, as well as the functions of the corresponding gene products.

References

Baba, M., K. Takeshige, N. Baba, and Y. Ohsumi. 1994. Ultrastructural analysis of the autophagic process in yeast: detection of autophagosomes and their characterization. *J. Cell. Biol.* 124:903–913.

Baba, M., M. Osumi, and Y. Ohsumi. 1995. Analysis of the membrane structures involved in autophagy in yeast by freeze-replica method. *Cell Struct. Funct.* 20:465–471.

Blommaart, E.F., U. Krause, J.P. Schellens, S.H. Vreeling, and A.J. Meijer. 1997. The phosphatidylinositol 3-kinase inhibitors wortmannin and LY294002 inhibit autophagy in isolated rat hepatocytes. *Eur. J. Biochem.* 243:240–246.

Bormann, C., and H. Sahm. 1978. Degradation of microbodies in relation to activities of alcohol oxidase and catalase in *Candida boidinii. Arch. Microbiol.* 117:67–72.

Chiang, H.-L., R. Schekman, and S. Hamamoto. 1996. Selective uptake of cytosolic, peroxisomal, and plasma membrane proteins into the yeast lysosome for degradation. *J. Biol. Chem.* 271:9934–9941.

Dunn, W.A., Jr. 1994. Autophagy and related mechanisms of lysosome-mediated protein degradation. *Trends Cell Biol.* 4:139–143.

Faber, K.N., J.A. Heyman, and S. Subramani. 1998. The AAA-family peroxins, PpPex1p and PpPex6p, interact with each other in an ATP-dependent manner and are associated with different subcellular membranous structures distinct from peroxisomes. *Mol. Cell. Biol.* 18:936–943.

Gould, S.J., D. McCollum, A.P. Spong, J.A. Heyman, and S. Subramani. 1992. Development of the yeast *Pichia pastoris* as a model organism for a genetic and molecular analysis of peroxisome assembly. *Yeast.* 8:613–628.

Harding, T.M., G.A. Hefner, M. Thumm, and D.J. Klionsky. 1996. Genetic and phenotypic overlap between autophagy and the cytoplasm to vacuole protein targeting pathway. *J. Biol. Chem.* 271:17621–17624.

Kovacs, A.L., A. Reith, and P.O. Seglen. 1982. Accumulation of autophagosomes after inhibition of hepatocytic protein degradation by vinblastine, leupeptin or a lysosomotropic amine. *Exp. Cell Res.* 137:191–201.

Marzella, L., and H. Glaumann. 1987. In Lysosomes, their role in protein breakdown. Academic Press, San Diego, CA. 319–367.

Monosov, E.Z., T.J. Wenzel, G.H. Lüers, J.A. Heyman, and S. Subramani. 1996. Labeling of peroxisomes with green fluorescent protein in living *P. pastoris* cells. *J. Histochem. Cytochem.* 44:581–589.

Noda, T., A. Matsuura, Y. Wada, and Y. Ohsumi. 1995. Novel system for monitoring autophagy in the yeast *Saccharomyces cerevisiae. Biochem. Biophys. Res. Commun.* 210:126–132.

Sakai, Y., and S. Subramani. 1997. Green fluorescent protein (GFP) fluorescence through the rhodamine channel after excitation using the FITC filter set. *Technical Tips Online* T01319.

Scott, S.V., G.A. Hefner, K.A. Morano, T. Noda, Y. Ohsumi, and D.J. Klionsky. 1996. Cytoplasm-to-vacuole targeting and autophagy employ the same machinery to deliver proteins to the yeast vacuole. *Proc. Natl. Acad. Sci. USA.* 93:12304–12308.

Scott, S.V., M. Baba, Y. Ohsumi, and D.J. Klionsky. 1997. Aminopeptidase I is targeted to the vacuole by a nonclassical vesicular mechanism. *J. Cell Biol.* 138:37–44.

Spong, A.P., and S. Subramani. 1993. Cloning and characterization of *PAS5*: a gene required for peroxisome biogenesis in the methylotrophic yeast *Pichia pastoris. J. Cell Biol.* 123:535–548.

Stack, J.H., and S.D. Emr. 1994. Vps34p required for yeast vacuolar protein sorting is a multiple specificity kinase that exhibits both protein kinase and phosphatidylinositol-specific PI3-kinase activities. *J. Biol. Chem.* 269:31552–31562.

Subramani, S. 1998. Components involved in peroxisome import, biogenesis, proliferation, turnover, and movement. *Physiol. Rev.* 78:1–18.

Takeshige, K., M. Baba, S. Tsuboi, T. Noda, and Y. Ohsumi. 1992. Autophagy in yeast demonstrated with proteinase-deficient mutants and conditions for its induction. *J. Cell Biol.* 119:301–311.

Thumm, M., R. Egner, B. Koch, M. Schlumpberger, M. Straub, M. Veenhuis, and D.H. Wolf. 1994. Isolation of autophagocytosis mutants of *Saccharomyces cerevisiae. FEBS Lett.* 349:275–280.

Titorenko, V.I., I. Keizer, W. Harder, and M. Veenhuis. 1995. Isolation and characterization of mutants impaired in the selective degradation of peroxisomes in the yeast *Hansenula polymorpha. J. Bacteriol.* 177:357–363.

Tsukada, M., and Y. Ohsumi. 1993. Isolation and characterization of autophagy-defective mutants of *Saccharomyces cerevisiae. FEBS Lett.* 333:169–174.

Tuttle, D.L., and W.A. Dunn, Jr. 1995. Divergent modes of autophagy in the methylotrophic yeast *Pichia pastoris. J. Cell Sci.* 108:25–35.

Tuttle, D.L., A.S. Lewin, and W.A. Dunn, Jr. 1993. Selective autophagy of peroxisomes in methylotrophic yeasts. *Eur. J. Cell Biol.* 60:283–290.

Veenhuis, M., W. Harder, J.P. van Dijken, and F. Mayer. 1981. Substructure of crystalline peroxisomes in methanol-grown *Hansenula polymorpha*: evidence for an in vivo crystal of alcohol oxidase. *Mol. Cell. Biol.* 1:949–957.

Veenhuis, M., A. Douma, W. Harder, and M. Osumi. 1983. Degradation and turnover of peroxisomes in the yeast *Hansenula polymorpha* induced by selective inactivation of peroxisomal enzymes. *Arch. Microbiol.* 134:193–203.

Vida, T.A., and S.D. Emr. 1995. A new vital stain for visualizing vacuolar membrane dynamics and endocytosis in yeast. *J. Cell Biol.* 128:779–792.

Wiemer, E.A.C., G. Lüers, K.N. Faber, T. Wenzel, M. Veenhuis, and S. Subramani. 1996. Isolation and characterization of Pas2p, a peroxisomal membrane protein essential for peroxisome biogenesis in the methylotrophic yeast *Pichia pastoris. J. Biol. Chem.* 271:18973–18980.

Yuan, W., D.L. Tuttle, Y.J. Shi, G.S. Ralph, and W.A. Dunn Jr. 1997. Glucose-induced microautophagy in *Pichia pastoris* requires the alpha-subunit of phosphofructokinase. *J. Cell Sci.* 110:1935–1945.